Scientific Research Publishing

Open Journal of Applied Sciences, 2025, 15(7), 2051-2073
https://www.scirp.org/journal/ojapps
ISSN Online: 2165-3925
ISSN Print: 2165-3917

Determination of the Geotechnical Parameters of Tohouè Silty Sand (Semè-Kpodji) for Its Use in Road Construction in Southern Benin

Kocouvi Agapi Houanou*, Koutchika Roger Danvi, Kpomagbé Serge Dossou, Emmanuel Olodo

Laboratory of Energy and Applied Mechanics (LEMA), Polytechnic School of Abomey-Calavi (EPAC), University of Abomey-Calavi (UAC), Abomey-Calavi, Republic of Benin
Email: *agapikh13@yahoo.fr

How to cite this paper: Houanou, K.A., Danvi, K.R., Dossou, K.S. and Olodo, E. (2025) Determination of the Geotechnical Parameters of Tohouè Silty Sand (Semè-Kpodji) for Its Use in Road Construction in Southern Benin. *Open Journal of Applied Sciences*, **15**, 2051-2073.
https://doi.org/10.4236/ojapps.2025.157135

Received: May 14, 2025
Accepted: July 18, 2025
Published: July 21, 2025

Abstract

Silty sands are the most abundant materials in the Littoral region of southern Benin used in road construction. These materials were once the most available in quantity and quality. Thus, this study was initiated to characterize the silty sands of Tohouè, a locality of Semè-Kpodji, for their use in road construction. To do this, an experimental study based on normative tests was used. The silty sand identification tests made it possible to determine the rate of particles with a diameter of less than 80 mm or 7.67%. The dry density is 1.95t/cm^3 with a water content of 8.20% OPM, then the organic matter content equal to 0.13% with a sand equivalent of 23.07%. Similarly, the mechanical tests carried out resulted in the determination of the CBR index evaluated at 44.00% for 95% OPM with a linear swelling of 0.15%, then the cohesion whose estimated value at 95% OPM is 1.03 ± 0.25 MPa and the friction angle is 28.66˚. Thus, the pre-consolidation stress is 22.00 MPa, the shear modulus varies from 64.941 kPa to 103.848 kPa and the Poisson's ratio varies from 0.392 to 0.484 while the oedometric modulus is 1684.91 MPa. In addition, the oedometric stress of silty sand is estimated at 58.07 MPa with a compression index of 0.046%. Similarly, the swelling index is 0.007% and the void index is 0.42%. As for Young's modulus, it varies from 51.129 MPa to 289.110 MPa. Ultimately, the analysis of the different results in accordance with the specifications of the CEBTP 1984 guide revised in 2019 shows that silty sand can only be used as a foundation layer, regardless of the type of pavement. Finally, these studies have shown that the soil is not very compressible and over-consolidated.

Keywords

Silty Sand, Cohesion, Stress, Shear Modulus, Poisson's Ratio

1. Introduction

The construction of road, hospital, commercial, airport, and port infrastructure is a determining factor in a nation's economic emergence. However, road construction absorbs significant quantities of aggregates [1]-[5]. This generates significant financial investments and significant direct and indirect pressures on the environment. To minimize construction costs and optimize the carbon footprint in road construction, the use of locally available materials such as silty sand, laterite, crushed granite, and earth from the bar is recommended [2] [3] [5] [6]. In southern Benin, silty sand is favored in road construction given its availability in the departments of Atlantique, Littoral, and Ouémè [7] [8].

This study is initiated to determine the geotechnical characteristics of Tohouè silty sand (Sèmè Kpodji) for its use in road construction. Specifically, it involves determining the physical parameters, namely grain size, density, cleanliness, organic matter content, clay-content, optimal water content and mechanical parameters such as CBR index, internal friction angle, cohesion, oedometric modulus, on the one hand and on the other hand, from a numerical approximation, determining Young's modulus and Poisson's ratio. The determination of these geotechnical parameters will make it possible to evaluate the potential of Tohouè silty sand (Sèmè-Kpodji) in order to define the layers of the road structure, such as the subgrade, foundation and/or base layers of flexible pavements, in which its use is possible.

2. Materials and Methods

2.1. Material

2.1.1. Tohoué Silty Sand

The silty sand, the subject of this study, comes from the Tohoué quarry in the Tohouè District, Sèmè-Kpodji Commune. The Commune of Sèmè-Kpodji is located between the parallels 6˚22' and 6˚28' of North latitude and the meridians 2˚28' and 2˚43' of East longitude. The location of the quarry is completed by **Figure 1** below.

Figure 2 shows the silty sand sampling area at Tohouè.

Table 1 below shows the geographical coordinates of the various survey wells, silty sand sampling points of Tohouè.

Figure 3 shows a silty sand quarry in Tohoué (a) and a pile (b) of said material.

2.1.2. Material for Characterizing Tohouè Silty Sand

The equipment used for geotechnical tests complies with the requirements of current standards.

For the sieving granulometric analysis test, the experimental device including the accessories necessary for its implementation is governed by standard NF P 94-056 [9]. **Figure 4** shows all of said equipment.

As for the test of the measurement of the weight water content, the experimental device complies with the standard NF P94-050 [10]. The material required for its production is illustrated in **Figure 5** below.

Source: https://www.google.com/carte consulted on 07/12/2024.

Figure 1. Location of the Tohouè quarry.

Source: https://earth.google.com accessed 7/15/2024.

Figure 2. Location of the sampling site.

(a) (b)

Figure 3. Silty sand of Tohouè. (a) Tohouè Silty Sand Quarry; (b) Tohouè silty sandpile.

Table 1. Coordinates of the Tohouè silty sand drilling wells.

Coordinates of the survey wells		
Points	**X**	**Y**
A (Access track points)	461360.250	709603.166
E	461401.456	109486.696
G	461477.575	709487.750
I	461544.049	709533.489
K	461600.021	709585.684
M	461667.195	709576.335
N	461471.071	709589.051
O	461595.121	709672.117
P	461393.123	709557.105

Well drilling points

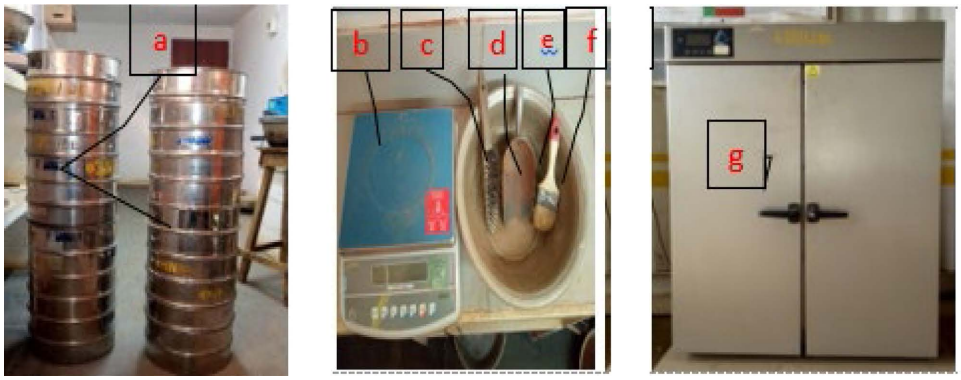

Legend :
a: Sieve series
b: Scale 30kg±0.2g
c: Brush
d: Main scoop
e: Brush
f: Container
g: Oven with adjustable temperature 50°C to 105°C ±2°C

Figure 4. Material for particle size analysis.

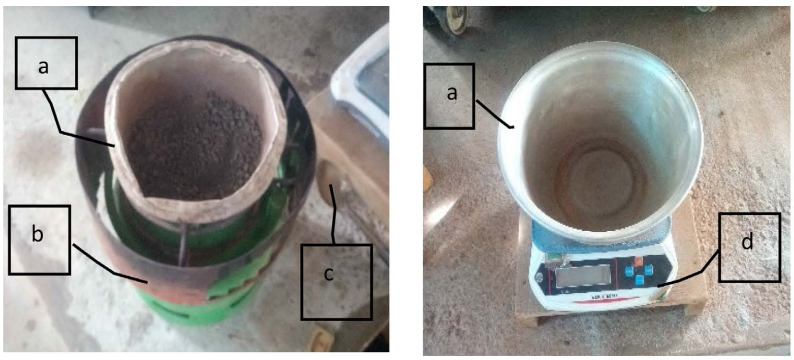

Legend :
a: Material bin
b: Gas burner
c: Ladle
d: Scale of 24kg±0.2g

Figure 5. Equipment for measuring water content.

For the test to determine the adsorption capacity of silty sand for methylene blue, the experimental device required for its implementation is prescribed by standard NF P 94-068 [11]. **Figure 6** below illustrates all of the said equipment.

For the test to determine the organic matter content on the silty sand of Tohouè, the experimental device set up complies with standard XP P 94-047 [12] as presented in **Figure 7** below.

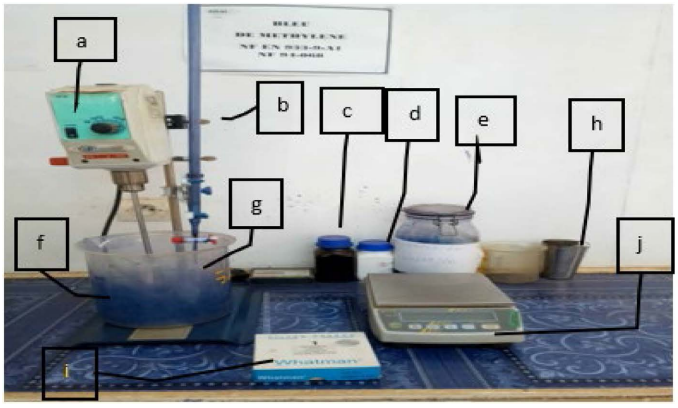

Legend :
a: Vane agitator
b: Stand
c: Yellow glass bottle
d: Dried kaolinite
e: Volumetric flask
f: Beaker
g: Oilcan
h: Methylene blue
i: White filter paper
j: Balance of 1000g±0.1g

Figure 6. Material for determining the methylene blue value.

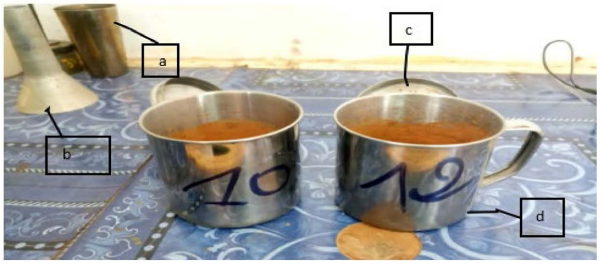

Legend :
a: Mortar
b: Pestle
c: Cover
d: Crucibles

Figure 7. Equipment for testing organic matter content.

Figure 8 below shows the different materials for determining the Sand Equivalent in the 0/2-mm fraction of sands. This test is carried out in accordance with AASHTO T176 [13], EN 933-8 [14].

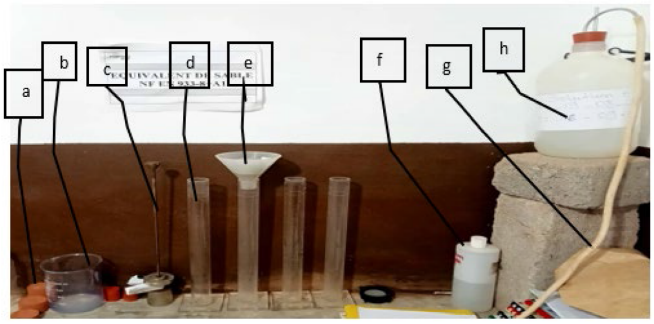

Legend :
a: rubber stoppers for test tube.
b: beaker;
c: 1 calibrated piston
d: plexiglass test tubes graduated at 100 and 380 mm
e: wide-necked funnel
f: measuring bottle capacity 200 ml.
g: 1 irrigator tube with tap and siphon.
h: 1000 ml of concentrated stock solution.

(a)

(b)

Figure 8. Material for the Sand Equivalent Test. (a) Equipment for determining sand equivalent; (b) Mechanical agitator.

Figure 9 below shows a set of experimental devices for carrying out the Modified Proctor test in accordance with standard NF P94-093 [15].

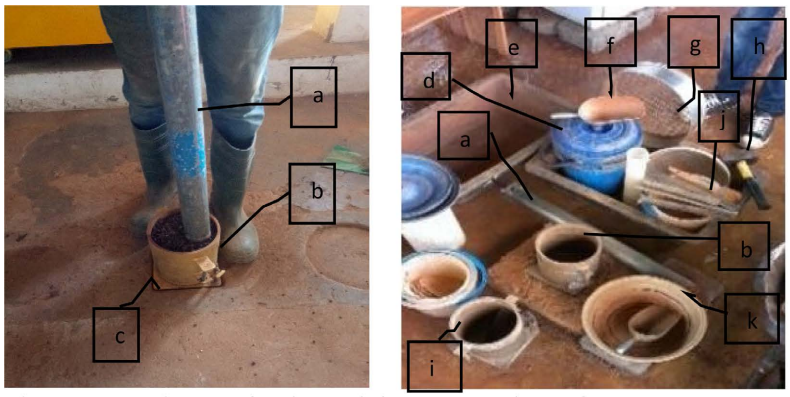

Legend :
a: Dame Proctor Modified
b: CBR mold
c: Base
d: Material bin
e: Plateau
f: Main scoop
g: Sieve
h: Hammer
i: Modified Proctor Mold
j: Accessories
k: Container

Figure 9. Equipment for determining compaction references.

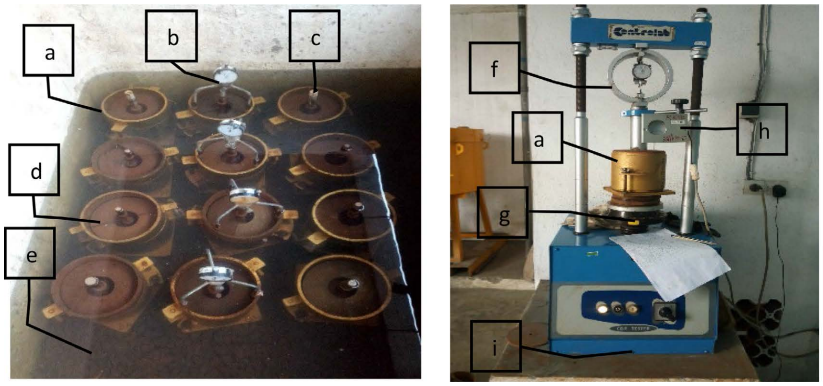

Legend :
a: CBR mold
b: Comparator
c: Overload series
d: Perforated metal disc
e: Immersion tank
f: Cadencentre
g: Risers
h: Comparator
i: CBR Press

Figure 10. Material for determining the CBR Bearing Index.

2.1.3. Geotechnical Test Equipment on the Tohouè Silty Sand

Figure 10 below shows a set of experimental devices for carrying out the CBR test in accordance with standard NF P94-078 [16].

Figure 11 shows a set of experimental devices for carrying out the rectilinear shear test on the box in accordance with standard NF EN ISO 17892-10 [17].

Figure 12 below shows the entire experimental device for carrying out the oedometric test according to standard XP P 94-091 [18].

2.2. Method

2.2.1. Method of Sampling Tohouè Silty Sand

Samples are taken in accordance with ISO 22475-1 [19].

2.2.2. Geotechnical Testing Method

The various geotechnical tests are carried out in accordance with the standards cited in §1.1.2.

Determination of the friction angle and internal cohesion by the Casagrande box shear the test, go through the calibration of the raw material from the initial condition through the values obtained from the Modified Proctor test, then

(a) (b)

Figure 11. Direct shear test equipment. (a) shear press; (b) Accesoires.

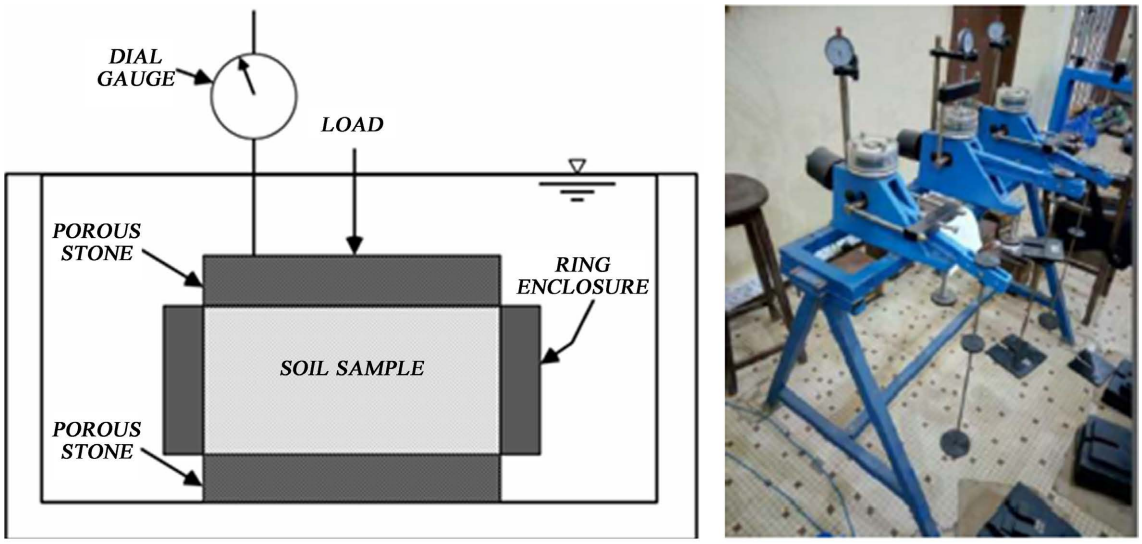

(a) (b)

Figure 12. Schematic design of an oedometer and oedometric testing apparatus. (a) Schematic design of an oedometer (source: Boo, 2019); (b) oedometric testing apparatus.

Step 1: Determination of the optimal water content and dry density on the material from the quarry (initial state).

Step 2: Determination of the optimal water content and dry density on the class 0/5 test sample.

Step 3: Carrying out the Casagrande box shears the test.

Step 4: Determination of the optimum water content and dry density on the test sample after the test.

2.2.3. Numerical Approach to Identifying the Parameters of the Hardin and Drnevich Hyperbolic Model

Previous studies have shown that the elastic behavior of soils is never linear in reality ([1] [20]). Therefore, it is important to focus studies on the nonlinear behavior of soils used in road construction. To do this, several mathematical models,

both hyperelastic and hypoelastic, can be used to describe these nonlinear behaviors of soils. However, it has been proven that hypoelastic models are the most recommended when it comes to small deformation studies. Two types of hypoelastic models exist, namely hyperbolic models and variable modulus models, as reported by Babaliyè in 2020. In the context of this study, hyperbolic models mathematically based on a representation of the stress-strain relationship using a hyperbolic or parabolic curve ([21]) are best suited to describe the nonlinear elastic behavior of soils ([1] [20]).

According to Hardin and Drnevich [22], the hypoelastic behavior of a material is given by Equation (1).

$$\tau = \frac{\gamma}{\frac{1}{G_{\max}} + \frac{\gamma}{\tau_{\max}}} \tag{1}$$

where $\tau_{\max}$ represents the maximum shear stress, $G_{\max}$ the maximum shear modulus, τ the shear stress and γ the shear strain.

To determine the parameters $\tau_{\max}$ and $G_{\max}$, Equation (1) was reformulated by setting: $a = 1/G_{\max}$ and $b = 1/\tau_{\max}$. which gives the following Equation (2):

$$\tau = \varphi(\gamma, a, b) = \frac{\gamma}{a + b\gamma}, \quad a, b \in \mathbb{R} \tag{2}$$

Using a nonlinear least fit method, the parameters a and b are evaluated. This method consists of fitting the experimental data y_i to the function φ by minimizing the distance φ_i between y_i. and $\varphi(\gamma, a, b)$:

$$\varphi_i = \sum_{i=1}^{n} \left[y_i - \varphi(\gamma, a, b) \right]^2 \tag{3}$$

The implementation of nonlinear regression follows the following steps:

1st Step: Linearization $\varphi(\gamma, a, b)$ of around (a_0, b_0)

$$\begin{cases} \dfrac{\partial \varphi}{\partial a}(\gamma, a, b) = -\dfrac{\gamma}{(a + b\gamma)^2} \\ \dfrac{\partial \varphi}{\partial b}(\gamma, a, b) = -\dfrac{\gamma^2}{(a + b\gamma)^2} \end{cases} \tag{4}$$

$$\varphi(\gamma, a, b) = \frac{\gamma}{a_0 + \gamma b_0} - \frac{\gamma}{(a_0 + b_0\gamma)^2}(a - a_0) - \frac{\gamma^2}{(a_0 + b_0\gamma)^2}(b - b_0) \tag{5}$$

Let us set: $A = \dfrac{\gamma}{(a_0 + b_0\gamma)^2}$; $B = \dfrac{\gamma^2}{(a_0 + b_0\gamma)^2}$ and $C = \dfrac{\gamma}{a_0 + b_0\gamma}$.

Equation (5) becomes:

$$\varphi(\gamma, a, b) = C - A(a - a_0) - B(b - b_0) \tag{6}$$

2nd Step: Determination of *a* and *b*.

The minimization of φ consists of canceling its first derivative with respect to the unknowns *a* and *b*. Let:

$$\begin{cases} \dfrac{\partial \varphi}{\partial a} = 0 \\ \dfrac{\partial \varphi}{\partial b} = 0 \end{cases} \tag{7}$$

With $\varphi(\gamma, a, b) = C - A(a - a_0) - B(b - b_0)$.

Development of the terms of the system of Equation (7).

Case of the first equation:

$$\frac{\partial \varphi_i}{\partial a} = 0 \Leftrightarrow \frac{\partial}{\partial a}\left[\sum \left(y_i - \varphi(\gamma, a, b)\right)^2\right] = 0 \tag{8}$$

$$\Leftrightarrow \sum \frac{\partial}{\partial a}\left(y_i - \varphi(\gamma, a, b)\right) \cdot \left(y_i - \varphi(\gamma, a, b)\right) = 0$$

$$\Leftrightarrow -\sum \frac{\partial}{\partial a}\varphi(\gamma, a, b) \cdot \left(y_i - \varphi(\gamma, a, b)\right) = 0$$

$$\Leftrightarrow -\sum (-A) \cdot \left(y_i - \varphi(\gamma, a, b)\right) = 0$$

$$\Leftrightarrow \sum A\left(y_i - C + A(a - a_0) + B(b - b_0)\right) = 0$$

$$\Leftrightarrow \sum Ay_i - \sum A \cdot C + \sum A^2 (a - a_0) + \sum A \cdot B(b - b_0) = 0$$

$$\Leftrightarrow (a - a_0)\sum A^2 + (b - b_0)\sum A \cdot B = \sum A \cdot C - \sum Ay_i$$

$$\Leftrightarrow (a - a_0)\sum A^2 + (b - b_0)\sum A \cdot B = \sum A(C - y_i) \tag{9}$$

Case of the second equation:

$$\frac{\partial \varphi_i}{\partial b} = 0 \Leftrightarrow \frac{\partial}{\partial b}\left[\sum \left(y_i - \varphi(\gamma, a, b)\right)^2\right] = 0 \tag{10}$$

$$\Leftrightarrow \sum \frac{\partial}{\partial b}\left(y_i - \varphi(\gamma, a, b)\right)\left(y_i - \varphi(\gamma, a, b)\right) = 0$$

$$\Leftrightarrow \sum \left(-\frac{\partial}{\partial b}\varphi(\gamma, a, b)\right) \cdot \left(y_i - C + A(a - a_0) + B(b - b_0)\right) = 0$$

$$\Leftrightarrow \sum -(-B)\left(y_i - C + A(a - a_0) + B(b - b_0)\right) = 0$$

$$\Leftrightarrow \sum B\left(y_i - C + A(a - a_0) + B(b - b_0)\right) = 0$$

$$\Leftrightarrow \sum \left(By_i - B \cdot C + A \cdot B(a - a_0) + B^2 (b - b_0)\right) = 0$$

$$\Leftrightarrow \sum B(y_i - C) + (a - a_0)\sum A \cdot B + (b - b_0)\sum B^2 = 0$$

$$\Leftrightarrow (a - a_0)\sum A \cdot B + (b - b_0)\sum B^2 = \sum B(C - y_i) \tag{11}$$

So we have the following system:

$$\begin{cases} (a - a_0)\sum A^2 + (b - b_0)\sum A \cdot B = \sum A(C - y_i) \\ (a - a_0)\sum A \cdot B + (b - b_0)\sum B^2 = \sum B(C - y_i) \end{cases} \tag{12}$$

Put into matrix form, the system of Equation (12) becomes:

$$\begin{pmatrix} \sum A^2 & \sum A \cdot B \\ \sum A \cdot B & \sum B^2 \end{pmatrix} \begin{pmatrix} a - a_0 \\ b - b_0 \end{pmatrix} = \begin{pmatrix} \sum A(C - y_i) \\ \sum B(C - y_i) \end{pmatrix} \tag{13}$$

Thus, the determinant ($\det M$) of this system of equations is:

$$\det M = \begin{vmatrix} \sum A^2 & \sum A \cdot B \\ \sum A \cdot B & \sum B^2 \end{vmatrix} \tag{14}$$

$$\Leftrightarrow \det M = \sum A^2 \sum B^2 - \sum A \cdot B \sum A \cdot B \tag{15}$$

Similarly, the determinants associated with a and b are det(a) and det(b) respectively.

Either:

$$\det(a) = \begin{vmatrix} \sum A(C - y_i) & \sum A \cdot B \\ \sum B(C - y_i) & \sum B^2 \end{vmatrix} \tag{16}$$

which is worth: $\det(a) = \sum A(C - y_i) \sum B^2 - \sum B(C - y_i) \sum A \cdot B$

$$\text{So,} \quad a - a_0 = \frac{\det(a)}{\det M}. \tag{17}$$

$$\text{That is:} \quad a = a_0 + \frac{\sum A(C - y_i) \sum B^2 - \sum B(C - y_i) \sum A \cdot B}{\sum A^2 \sum B^2 - \sum A \cdot B \sum A \cdot B} \tag{18}$$

Also,

$$\det(b) = \begin{vmatrix} \sum A^2 & \sum A(C - y_i) \\ \sum A \cdot B & \sum B(C - y_i) \end{vmatrix} \tag{19}$$

which gives: $\det(b) = \sum A^2 \sum B(C - y_i) - \sum A \cdot B \sum A(C - y_i)$

$$\text{So,} \quad b - b_0 = \frac{\det(b)}{\det M} \tag{20}$$

$$\text{Consequently,} \quad b = b_0 + \frac{\sum A^2 \sum B(C - y_i) - \sum A \cdot B \sum A(C - y_i)}{\sum A^2 \sum B^2 - \sum A \cdot B \sum A \cdot B} \tag{21}$$

The following system is made up:

$$\begin{cases} a = a_0 + \dfrac{\sum A(C - y_i) \sum B^2 - \sum B(C - y_i) \sum A \cdot B}{\sum A^2 \sum B^2 - \sum A \cdot B \sum A \cdot B} \\ b = b_0 + \dfrac{\sum A^2 \sum B(C - y_i) - \sum A \cdot B \sum A(C - y_i)}{\sum A^2 \sum B^2 - \sum A \cdot B \sum A \cdot B} \end{cases} \tag{22}$$

From a Python program, the optimal value of each parameter a and b of Equation (22) is determined by respecting the stopping criterion defined by Equation (23) (Montgomery and Runger, [23]; Houanou, [24]; Babaliye, [1]).

$$\frac{a - a_0}{a_0} < 10^{-6} \tag{23}$$

2.2.4. Evaluation of Young's Modulus (E) and Poisson's Ratio (ν)

According to Gérard Degoutte and Paul Royet (2007) and Leipholz [25], the calculation of Young's modulus (E) and Poisson's ratio (υ) can be done from oedometric and shear tests. Thus, the following Equations (24) and (25) are used:

$$E = 2G(1+\upsilon) \tag{24}$$

$$E = E_{oed}\frac{(1+\upsilon)(1-2\upsilon)}{1-\upsilon} \tag{25}$$

where we denote by:

G, the shear modulus,

E, the Young's modulus,

υ, Poisson's ratio,

E_{oed}, the oedometric module.

Equations (24) and (25) allowed us to obtain the following Equation (26):

$$2G(1+\upsilon) = E_{oed}\frac{(1+\upsilon)(1-2\upsilon)}{1-\upsilon} \tag{26}$$

Thus, the transformation of Equation (26) becomes:

$$\upsilon = \frac{E_{oed}-2G}{2(E_{oed}-G)} \tag{27}$$

Furthermore, the determination of the oedometric modulus is obtained by Equation (28):

$$E_{oed} = \frac{1+e_0}{C_c}\frac{\sigma'_{final}-\sigma'_{initial}}{\log\left(\frac{\sigma'_{final}}{\sigma'_{initial}}\right)} \tag{28}$$

with

e_0, Index of voids in the soil in place,

C_c, Compression index of the soil in place,

$\sigma'_{initial}$, Initial normal stress,

σ'_{final}, Final normal stress.

3. Results and Discussions

3.1. Results

T results from experimental tests carried out on a series of samples of Tohouè silty sand are as follows:

3.1.1. Results of the Sieving Granulometric Analysis Test

The samples from the loan were subjected to a granulometric analysis by sieving, Figure 13 below shows the different granulometric curves.

From the curves in Figure 13 below, different parameters are evaluated and the results are recorded in Table 2 below.

From the analysis of Table 2, it appears that the curvature coefficient C_c is between 1 and 3. Thus, according to the NF P 94-056 [9] standard, the grain size is well spread, therefore, the Tohouè silty sand is well graduated. In addition, the uniformity coefficient is between 2 and 5. It can be deduced that the grain size of said silty sand is spread according to the NF P 94-056 [9] standard. In conclusion, the Tohouè silty sand has a spread grain size.

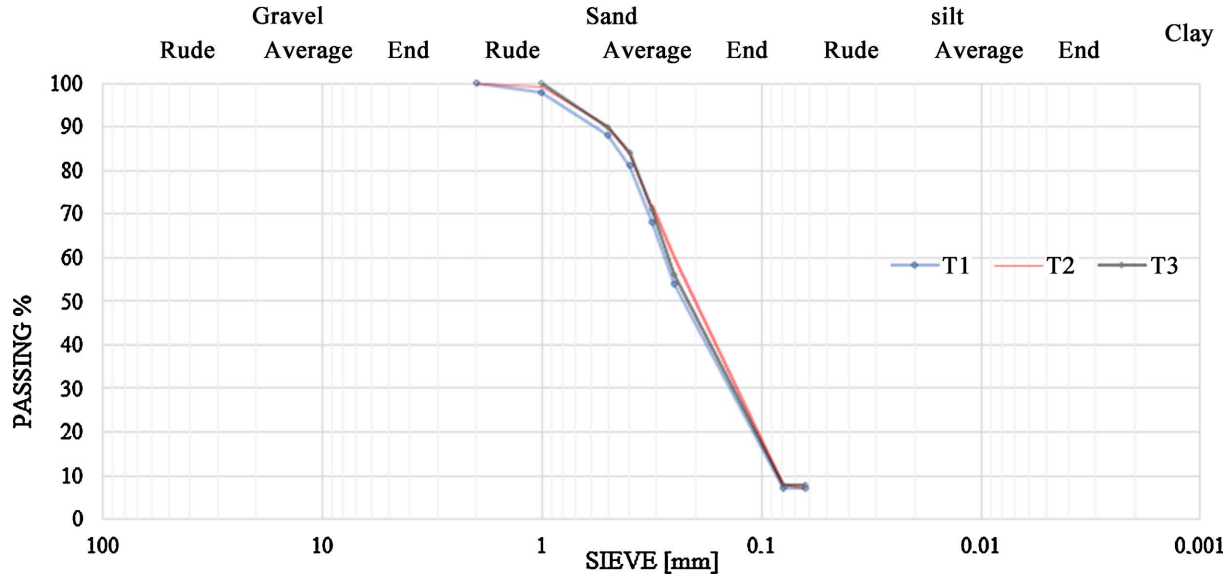

Figure 13. Granulometric curves of silty sand.

Table 2. Results of the sieving granulometric analysis test.

	D_{max}	$D_{0.08}$	$D_{0.063}$	D_{10}	D_{30}	D_{60}	C_C	C_U
Sample 1	2.00	7.00	7.00	0.09	0.16	0.28	1.02	3.11
Sample 2	2.00	8.00	7.00	0.09	0.15	0.25	1.00	2.78
Sample 3	2.00	8.00	8.00	0.09	0.16	0.27	1.05	3.00

Table 3. Organic matter content of Tohouè silty sand.

Designation	Sample 1	Sample 2	Sample 3	Mean	Standard deviation
Organic matter content (%)	0.13	0.15	0.11	0.13	0.02

The percentage at the 0.080-mm sieve pass is 7.67%. This value obtained is lower than those determined by P'Kla *et al.* [26], *i.e.* 12% to 34%, and Tankpinou *et al.* [7], *i.e.* 18.52%. Thus, the silty sand of Tohouè contains fewer fine elements.

3.1.2. Organic Matter Content

The determination of the organic matter content carried out on the silty sand samples gave the results listed in the following **Table 3**.

According to **Table 3**, the Tohouè sand has a mean organic matter content of 0.13% less than 1.5%, which means that the material is weakly organic [12].

3.1.3. Methylene Blue Value

The results of the methylene blue value are recorded in **Table 4** below:

Table 4. Methylene blue value on silty sand.

Designation	Sample 1	Sample 2	Sample 3	Mean	Standard deviation
VBS (%)	0.35	0.41	0.46	0.41	0.06

From the analysis of this table, it appears that the methylene blue value of silty sand is 0.41%, between 0.2 and 1.5. Thus, the silty sand of Tohouè is of the sandy-silty type according to standard NF P 94-068 [11].

3.1.4. Sand Equivalent Value

The results of the Sand Equivalent test on the Tohouè silty sand are recorded in Table 5 below:

Table 5. Sand equivalent value on the silty sand of Tohouè.

Designation	Sample 1	Sample 2	Sample 3	Mean	Standard deviation
ES (%)	23.3	22.2	23.7	23.07	0.78

The results from Table 5 show that the Sand Equivalent value of Tohouè silty sand is 23.07%, lower than 60%. Thus, Tohouè silty sand is classified as sandy-clayey with a risk of potential shrinkage or swelling according to AASHTO T176 [13], EN 933-8+A1 [14].

3.1.5. Proctor Test Results

These results are presented in the form of a curve with the optimal water content on the abscissa and the maximum dry density on the ordinate (see Figure 14).

The results obtained for this test are contained in Table 6 below:

From this table, it appears that the value of the maximum dry density of the

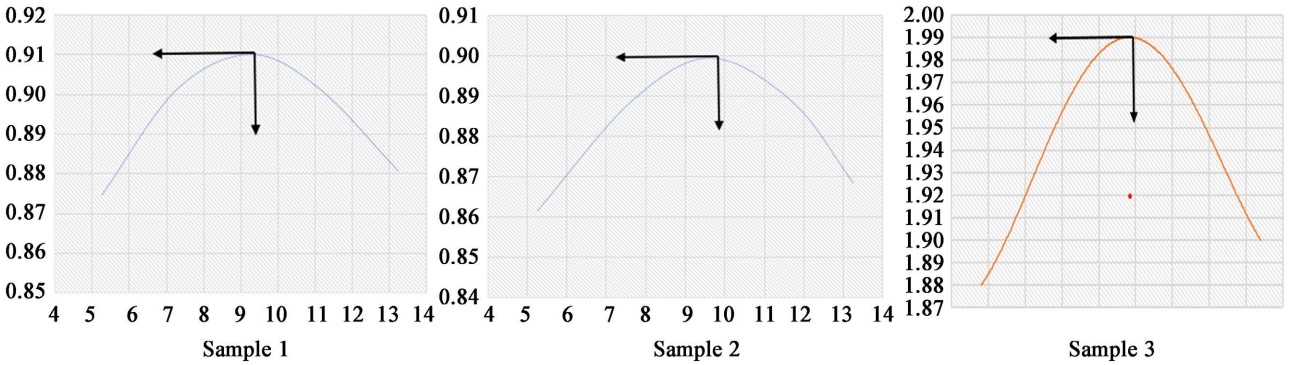

Figure 14. Modified Proctor curve of natural silty sand.

Table 6. Results of Modified Proctor, CBR and Swelling tests on silty sand.

Samples	Modified Proctor		Swelling	CBR		
	γ_d (t/m^3)	w (%)	w (%)	90%	95%	100%
Test 1	2.02	6.5	0.11	26	47	81
Test 2	1.99	8.9	0.17	16	45	70
Test 3	1.85	9.2	0.16	12	40	69
Mean	1.95	8.20	0.15	18.00	44.00	73.33
Standard deviation	0.09	1.48	0.03	7.21	3.61	6.66

Tohouè silty sand determined at the Modified Proctor Optimum is 1.95 t/m^3, a value lower than that determined by Tankpinou *et al.* [7], *i.e.* 2.02 t/m^3.

3.1.6. California Bearing Ratio (CBR) Test Results

The punching measurements carried out on nine (09) specimens divided into three (03) series according to the molds, are recorded in **Table 6** as well as the values of the linear swelling of the specimens. The analysis of the CBR data shows that the CBR index increases when the density increases. The improvement in the CBR is due to the reduction of voids within the sample after compaction.

The CBR index determined for the Tohouè silty sand has a value of 44% to 95% of the OPM (**Table 6**). This value obtained is between the values of the CBR indices determined by P'Kla *et al.* (2016) on similar soil types, *i.e.* 23% and 49%. On the other hand, it is higher than that obtained by Tankpinou *et al.* [7], *i.e.* 3.00%, also on silty sands.

Houngue's [27] work demonstrated that silty soils with a CBR around 40-50% are often used for subgrades, particularly in tropical climates where humidity varies significantly. He also suggested that stabilizing these soils not only improves the CBR but also durability under climatic conditions.

Similarly, Agossou (2017), studying various soils of Benin including the silty sand of Tohouè, concluded that with a CBR of 44%, these soils can be used as subgrade for moderate traffic roads, but it would be better to stabilize them for higher traffic roads.

As for the linear swelling coefficient of Tohouè silty sand, it is of the order of 0.15%. This linear swelling rate is considered relatively low CEBTP [28]. It indicates that silty sand is not particularly subject to significant dimensional variations in response to variations in water content. This allows us to conclude that Tohouè silty sand has low swelling. This low linear swelling is necessary to ensure the stability and durability of a roadway structure.

3.1.7. Direct Shear Test (NF EN ISO 17892-10)

Table 7 gives the average values of dry density and optimum content on the run-of-mine material, the calibrated material before and after the shear test. These values are determined to specify the test conditions.

The values obtained made it possible to plot the tangential stresses as a function of the displacement (**Figure 15(a)** and **Figure 15(b)**), on the one hand, and on

Table 7. Values of water content and dry density on the material at different stages.

Type of materials	Essay	No. 1	No. 2
All comers	ω_{OPM} (%)	8.20	7.25
	γ_d (kN/m^3)	1.95	1.99
Calibrated material	$\omega_{initiale}$ (%)	5.42	7.7
	γ_d (kN/m^3)	19.64	18.14
Material after shear test	ω_{finale} (%)	16.32	16.37

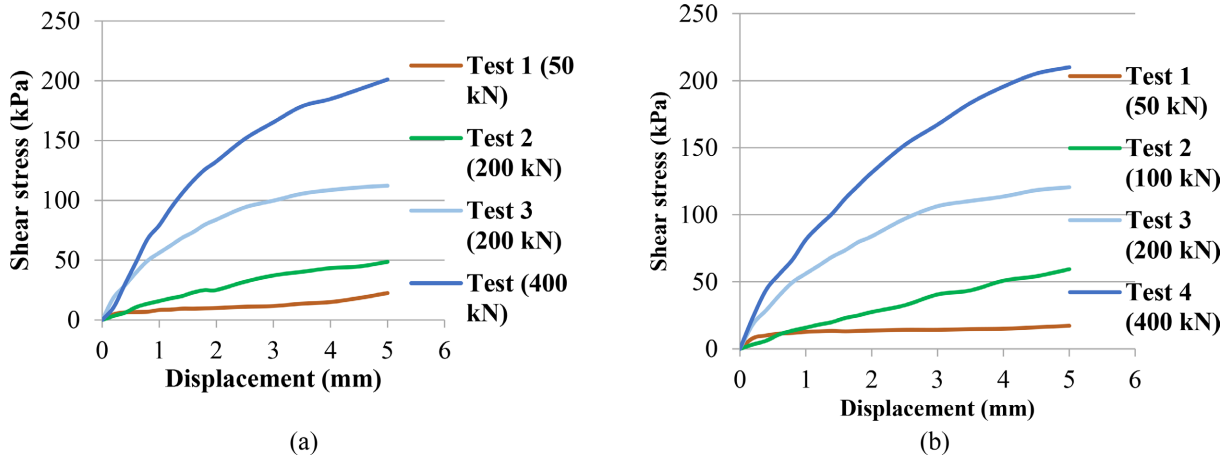

Figure 15. Shear stress versus displacement curves. (a) Test No. 1; (b) Test No. 2.

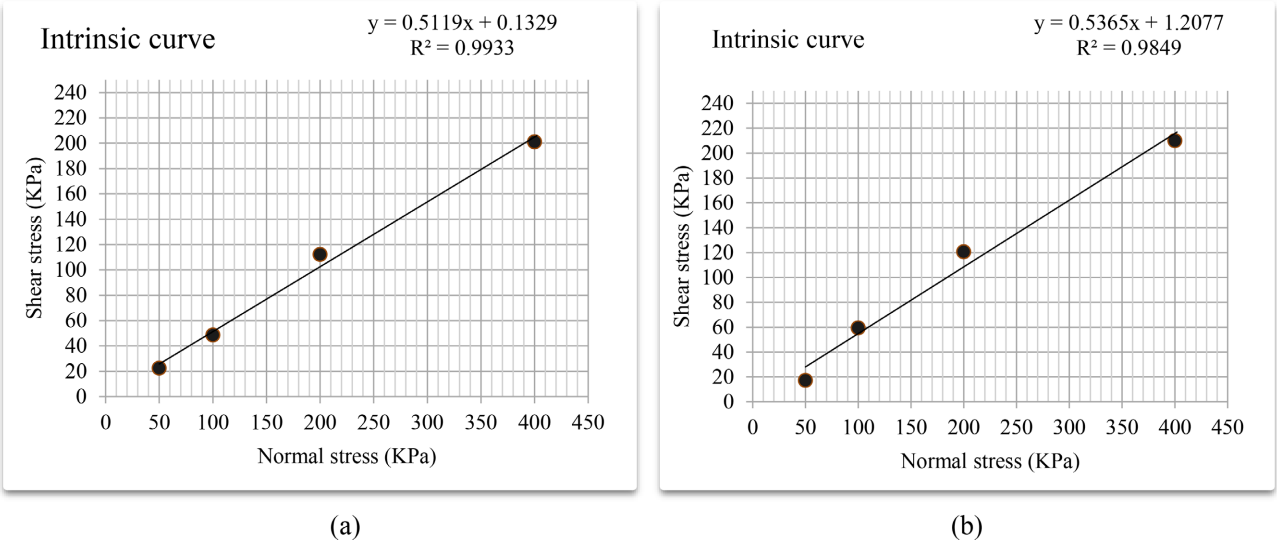

Figure 16. Shear stress versus normal stress curve. (a) Test No. 1; (b): Test No. 2.

the other hand, the shear stress as a function of the normal stress (Figure 16(a) and Figure 16(b)).

From the analysis of Figure 15, it appears that the curve of the test 1, carried out with a normal stress of 50 kPa, is below that of test 2 relating to a normal stress of 100 kPa. This trend is observed with tests 3 and 4 carried out respectively with a normal stress of 200 kPa and 400 kPa. However, this trend is reversed shortly after the start of the test just before the millimeter of displacement when considering the case of tests 1 and 2, on the one hand, and on the other hand, that of tests 3 and 4. This phenomenon may be due to a reorganization of the material. Also, the same phenomenon is observed on the evolution of the shear stress with the increase of the applied load.

Analyzing Figure 16, we see that the tangential stress evolves in the same direction as the normal stress. We note that the slope reflecting this increase is of the order of 0.500. The equation of the typical Coulomb line of a shear test is of the

form: $\tau = c + \sigma \tan \varphi$ where τ shear stress; c the cphesion; σ normal stress and φ internal friction angle.

By identification, the equations of the line from tests 1 and 2 (Figure 16) made it possible to give the values of c and φ recorded in Table 8.

According to Table 8, we note that the internal friction angle of the Tohouè silty sand is 27.66˚ against 0.54 kPa for internal cohesion.

3.1.8. Oedometric Test ([18])

The results of the oedometric test made it possible to plot the following oedometric curves:

Table 9 lists the parameters taken from the oedometric test using the oedometric curve (Figure 17).

Table 8. Shear characteristics of silty sand.

Designation	c (kPa)	φ (˚)
Test 1	0.1329	1
Test 2	1.2077	28.21
Mean	0.5374	0.66
Standard deviation	1.0746	1.10

Table 9. Average results of oedometric testing carried out on specimens of silty soils from Tohouè.

N˚	e_o	$\sigma_{p'}$ (kPa)	c_c	c_g	γ_d (g/cm ^{3})	γ_h (g/cm ^{3})
Test 1	1.14	22.0	0.046	0.12	1.86	1.96
Test 2	1.14	22.0	0.046	0.12	1.86	1.95
Mean	1.14	22.0	0.046	0.12	1.86	1.95
Standard deviation	0	0	0	0	0	0.007

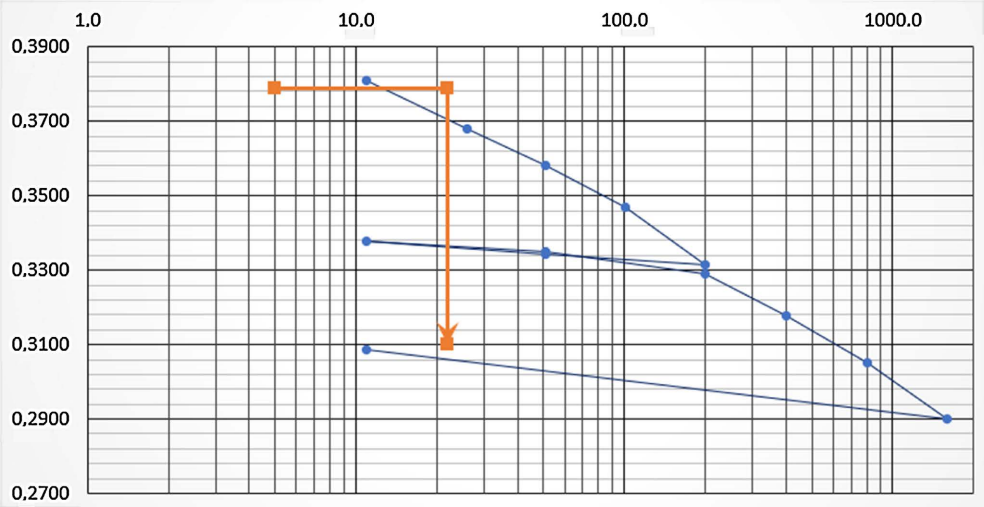

Figure 17. Oedometric compressibility curve at 95% OPM.

From the analysis of this table, we see that all the determined parameters are constant with the exception of the wet density.

The evaluation of the report $\frac{C_C}{1+e_0}=0.022$ showed that the silty sand of Tohouè is not very compressible ([29]). This behavior of the material may be due to its low fine particle content which is around 7.47%.

Furthermore, the swelling coefficient is 0.12%, less than 1%. Consequently, the silty sand of Tohouè is not swelling.

3.2. Modeling of Hypoelastic Behavior

3.2.1. Development and Validation of Numerical Models

The successive iterations, carried out from the equation system (11) led to the determination of the optimal value of the parameters of the Hardin Drnevich numerical model. These different values are presented in Table 10 below. They concern the normal stress, the shear modulus and the shear stress.

Table 10. Summary of the optimal values of the parameters G_{max} and τ_{max}.

Normal stress (kPa)	50		100		200		400	
Paramètres	G_{max}	τ_{max}	G_{max}	τ_{max}	G_{max}	τ_{max}	G_{max}	τ_{max}
Sample 1	64,941	15,944	18,351	103,190	92,608	152,561	103,063	341,076
Sample 2	64,942	15,944	16,083	220,914	84,432	172,323	104,634	358,990
Mean	64,941	15,944	17,217	162,052	88,520	162,442	103,848	350,033

Figures 18(a)-(d) and Figures 19(a)-(d) below represent the Hardin and Drnevich hyperbolic behavior curves of the soil from the Tohouè silty sand.

We observe that the stress-strain curves of the model are very close to those of the observations. Thus, we can say that the model fits the observations well.

3.2.2. Model Adequacy Test: Calculation of the Coefficient of Determination

Table 11 shows the different values of the calculated coefficient of determination.

According to Table 11, the coefficients of determination of each compaction energy are close to 100% (varies from 91.99% to 99.40%) except for sample 1 at 50 kPa, this observation may be due to a reworking of the material during the test or a relaxation. This clearly shows that the Hardin and Drnevich model are adequate.

3.3. Determination of Oedometric Stress

Table 12 presents the results of the oedometric test evaluated on the silty sand of Tohouè.

These results show that the soil studied has low compressibility as the C_c is less than 0.2 according to the NF EN ISO 17892-5 [30] standard and good resistance to deformation under applied loads, which is favorable for its use in construction applications where significant loads can be expected.

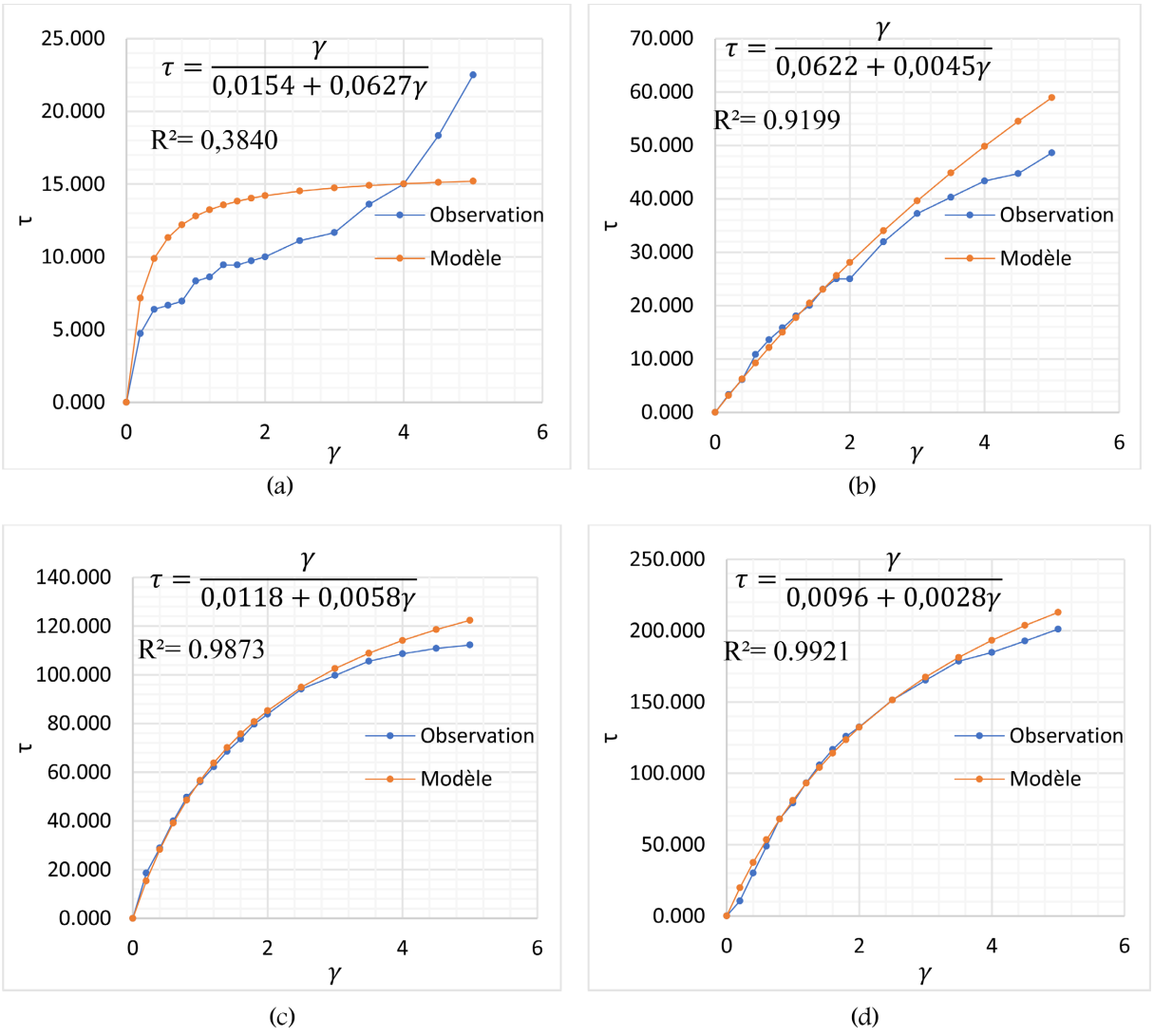

Figure 18. Shear stress as a function of deformation of Tohouè silty sand for sample 1. (a) 50 kPa normal stress case; (b) 100 kPa normal stress case; (c) 200 kPa normal stress case; (d) Normal stress case of 400 kPa.

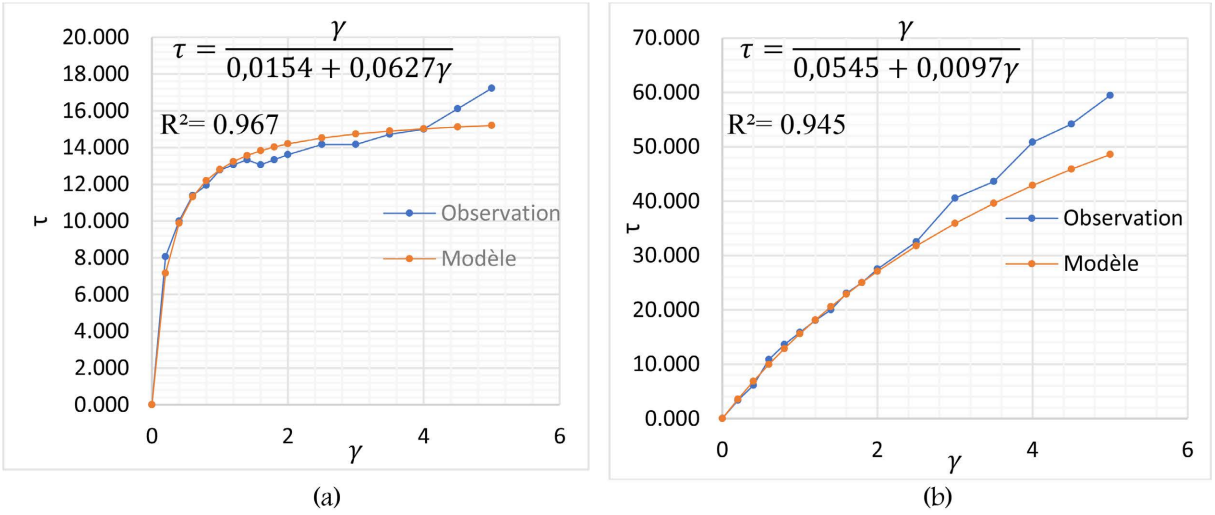

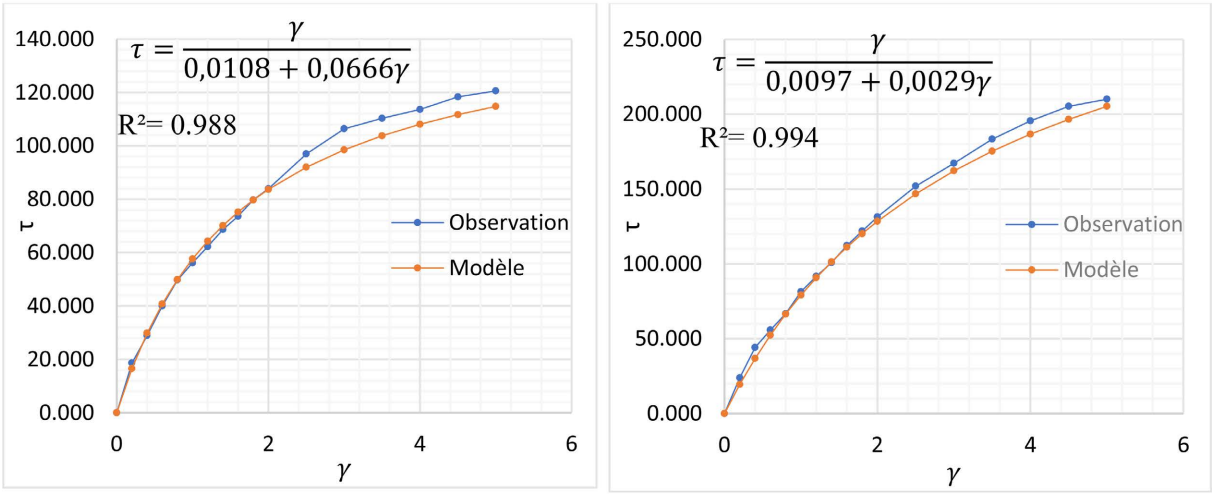

Figure 19. Shear stress as a function of deformation of Tohouè silty sand for sample 2. (a) 50 kPa normal stress case; (b) 100 kPa normal stress case; (c) 200 kPa normal stress case; (d) Normal stress case of 400 kPa.

Table 11. Values of the calculated coefficient of determination.

Normal Stresses (kPa)		50	100	200	400
Sample 1	R^2 (%)	38.40	91.99	98.73	99.21
Sample 2		96,67	94.49	98.81	99.40

Table 12. Value of oedometric stress.

e_0	C_c	$\sigma'_{initial}$ (kPa)	σ'_{final} (kPa)	$\log\left(\sigma'_{final} - \sigma'_{initial}\right)$	E_{oed} (MPa)
0.42	0.046	101	1601.2	1.2	58.07

Table 13. Values of Poisson's ratio and Young's modulus of silty sand.

Normal Stresses	σ_n (kPa)	50	100	200	400
Maximum shear modulus	G_{max} (kPa)	64,941	17,217	88,520	103,848
Poisson's ratio	υ	0.438	0.485	0.411	0.392
Young's modulus (MPa)	E	186,707	51,129	249,761	2891.10

3.4. Determination of Poisson's Ratio and Young's Modulus

Table 13 below gives the Poisson's ratios and Young's moduli derived respectively from Equations (24)-(27) and (24) or (25).

The analysis of this Table 13 shows that the shear modulus varies from 64.941 kPa to 103.848 kPa and the Poisson's ratio varies from 0.392 to 0.484 while the Young's modulus varies from 51.129 MPa to 289.110 MPa. We note a decrease in the Poisson's ratio with the increase in normal stress like the normal stress at 50 kPa. In addition, the shear modulus and the Young's modulus increase with the normal stress at different applications.

3.5. Discussion

Analysis of the data in Table 14 shows that the material contains little water because its average water content, 3.5%, is less than 4%. In fact, according to the NF P 94-093: [15] standard, this material is good for compaction.

Table 14. Summary of the geotechnical characteristics of silty sand facing the CEBTP [28] 1984 thresholds revised [31].

Features	Values of silty sand	CEBTP1984 thresholds revised 2019	
		Foundation layer	Base layer
Percentage passing through the 80 µm sieve (%)	7.67%	<35	<20
Dry density OPM (t/m³)	1.95	≥1.8 - 2.00	≥2.0
Linear swelling index (%)	0.15	<1.00	<1.00
CBR Index at 95% OPM (%)	44.00	≥30	≥80
Organic matter rate (%)	0.13	≤1%	≤1%
Methylene Blue Value (%)	0.41	≥0.2 - 8.0	≥0.2 - 8.0
Optimum water content (%)	8.20	≥7 and ≤13%	≥7 and ≤13%

Table 15. Verification of silty sand parameters at the foundation layer thresholds.

Features	Values of silty sand	CEBTP1984 thresholds revised 2019	
		Foundation layer	Compliance
Percentage passing through the 80 µm sieve (%)	7.67%	<35	Yes
Dry density OPM (t/m³)	1.95	≥1.8 - 2.00	Yes
Linear swelling index (%)	0.15	<1.00	Yes
CBR Index at 95% OPM (%)	44.00	≥30	Yes
Organic matter rate (%)	0.13	≤1%	Yes
Methylene Blue Value (%)	0.41	≥0.2 - 8.0	Yes
Optimum water content (%)	8.20	≥7 and ≤13%	Yes

According to this Table 15, the silty sand of Tohouè meets all the criteria for use as a foundation layer for flexible pavements.

According to this Table 16, Tohouè silty sand does not meet all the criteria for use as a base layer for flexible pavements. To use it as a base layer, it is necessary to make an improvement, either by cement stabilization, litho-stabilization, or other means.

4. Conclusions

The aim of this study is to determine the geotechnical characteristics of Tohouè

Table 16. Verification of silty sand parameters at the base layer thresholds.

Features	Values of silty sand	CEBTP1984 thresholds revised 2019	
		Base layer	**Compliance**
Percentage passing through the 80 µm sieve (%)	7.67%	<20	Yes
Dry density OPM (t/m^3)	1.95	≥2.0	No
Linear swelling index (%)	0.15	<1.00	Yes
CBR Index at 95% OPM (%)	44.00	≥80	No
Organic matter rate (%)	0.13	≤1%	Yes
Methylene Blue Value (%)	0.41	≥0.2 - 8.0	Yes
Optimum water content (%)	8.20	≥7 and ≤13%	Yes

silty sand for its use in road construction. Based on standard tests and in accordance with the thresholds of CEBTP [28] amended [31], they have shown that Tohouè silty sand can be used as a subgrade but not as a base layer for flexible pavements. In order to use it as a base layer, it is important to improve it by adding another material of better quality.

From the direct shear test, the oedometric test and the Hardin Drnevich numerical model, this study made it possible to determine the value of the Poisson's ratio which is 0.4 greater than 0.2 used by default.

By the same approach, the values of the shear modulus (64.941 kPa; 17.217 kPa; 88.520 kPa; 103.848 kPa) and the Young's modulus (186.707 kPa; 51.129 kPa; 249.761 kPa; 289.110 kPa) are respectively for an applied normal stress of 50 kPa, 100 kPa, 200 kPa, 400 kPa.

The approach used here is a simple original approach which makes it possible to determine the values of certain parameters initially taken by default in the absence of suitable equipment.

Conflicts of Interest

The authors declare no conflicts of interest regarding the publication of this paper.

References

[1] Babaliye, O. (2020) Comportement élastique non linéaire des mélanges de graves latéritiques et du concassé granitique non liés en couche support des chaussées souples. PhD Thesis, EPAC/UAC.

[2] Dossou, S.K. (2023) Valorisation en technique routière de la grave latéritique de Avlamè en République du Bénin. PhD Thesis, EPAC/UAC.

[3] Houanou, K.A., Dossou, K.S., Prodjinonto, V., Ahouétohou, P. and Olodo, E. (2022) Mechanical Characteristics of Avlamè Lateritic Gravel Improved with Granite Crushed for Its Use in Road Construction in Benin. *World Journal of Advanced Research and Reviews*, **15**, 279-292. https://doi.org/10.30574/wjarr.2022.15.2.0820

[4] Houanou, K.A., Dossou, K.S., P'kla, A., Prodjinonto, V., Adjagboni, C.E. and Olodo,

E. (2022) Technical Parameters of the Cana-Atchia Lateritic Aggregate for Its Use in Road Engineering in Southern Benin. *Current Journal of Applied Science and Technology*, **41**, 21-33. https://doi.org/10.9734/cjast/2022/v41i2031746

[5] Adjagboni, C.E. (2021) Détermination des paramètres mécaniques et thermophysiques d'un matériau routier granulaire non lié. Mémoire de Master Recherche, ES-DSI/UAC.

[6] Mahougbe, C.D.A. (2021) Analyse du cycle de vie des chaussées à base de la grave latéritique d'avlamè crue ou stabilisée. Mémoire d'Ingénieur de conception, EPAC/UAC.

[7] Tankpinou, K.Y., Gbaguidi, V. and Zèvounou, C. (2013) Mise au point pour assises de chaussées de matériaux élaborés (Sable silteux et concassés). *Journal de la Recherche Scientifique de l'Université de Lomé* (*Togo*) (*JRSUL*), **15**, 143-149.

[8] P'Kla, A. (2002) Caractérisation en compression simple des blocs de terre comprimée (BTC): Application aux maçonneries "BTC-mortier de terre". PhD Thesis, INSA. https://theses.fr/2002ISAL0037

[9] NFP 94-056 (1996) Sols: Reconnaissance et essais—Analyse granulométrique-Méthode par tamisage à sec après lavage. Association Française de Normalisation.

[10] NF P94-050 (1991) Sols : Reconnaissance et essais—Détermination de la teneur en eau pondérale des sols-Méthode par étuvage. Association Française de Normalisation.

[11] NF P94-068 (1998) Sols: Recherche et essais—Mesure de la capacité d'adsorption du bleu de méthylène d'un sol rocheux. Détermination du bleu de méthylène d'un sol par essai de déformation. Association Française de Normalisation.

[12] XP P94-047 (1998) Sols: Reconnaissance et essais—Détermination de la teneur pondérale en matières organiques d'un matériau-Méthode par calcination. Association Française de Normalisation.

[13] Aashto T176-16 (2016) Plastic Fines in Graded Aggregates and Soils by Use of the Sand Equivalent Test. 4.

[14] NF EN 933-8+A1 (2015) Essais pour déterminer les caractéristiques géométriques des granulats—Partie 8: Evaluation des fines—Équivalent de sable. Afnor EDITIONS.

[15] NF P94-093 (2014) Sols: Reconnaissance et essais—Détermination des références de compactage d'un matériau—Essai proctor normal—Essai proctor modifié. Afnor EDITIONS.

[16] NF P94-078 (1997) Sols: Reconnaissance et essais-indice CBR après immersion, indice CBR immédiat indice portant immédiat-mes. Sur échantilllon compacté dans moule CBR. Association Française de Normalisation.

[17] NF EN ISO 17892-10 (2018) Reconnaissance et essais géotechniques—Essais de laboratoire des sols—Partie 10 : Essai de cisaillement direct. Association Française de Normalisation.

[18] XP P94-091 (1995) Sols: Reconnaissance et essais—Essai de gonflement à l'oedomètre—Détermination des déformations par chargement de plusieurs éprouvette. AFNOR, 13.

[19] ISO 22475-1 (2021) Reconnaissance et essais géotechniques—Méthodes de prélèvement et mesurages piézométriques Partie 1: Principes techniques pour le prélèvement des sols, des roches et des eaux souterraines. ISO.

[20] Babaliye, O. Houanou, K.A., Godo, A.L.A., Tchehouali, A., Vianou, A. and Foudjet, A.E. (2019) Non-Linear Elastic Behavior of Lateritic Gravelly Road Material of Benin. *Journal of Materials Science & Surface Engineering*, **6**, 876-880. https://www.jmsse.in/files/655_%20Olivier%20et%20al.pdf

[21] Kondner, R.L. (1963) Hyperbolic Stress-Strain Response: Cohesive Soils. *Journal of*

the Soil Mechanics and Foundations Division, **89**, 115-143. https://doi.org/10.1061/jsfeaq.0000479

[22] Hardin, B.O. and Drnevich, V.P. (1972) Shear Modulus and Damping in Soils: Design Equations and Curves. *Journal of the Soil Mechanics and Foundations Division*, **98**, 667-692. https://doi.org/10.1061/jsfeaq.0001760

[23] Montgomery, D.C. and Runger, G.C. (2003) Applied Statistics and Probability for Engineers. John Wiley & Son.

[24] Houanou, K.A. (2014) Comportement differe du materiau bois, vers une meilleure connaissance des parametres viscoelastiques lineaires. Thèse, Université d'Abomey-Calav.

[25] Leipholz, H.H.E. (1974) On Conservative Elastic Systems of the First and Second Kind. *Ingenieur-Archiv*, **43**, 255-271.

[26] P'Kla, A., Amey, K.B. and Neglo, K. (2016) Caractérisation géotechnique du sable silteux utilise en couche de chaussée au sud du Togo et du Benin. *Journal de la Recherche Scientifique de l' Université de Lomé* (*Togo*) (*JRSUL*), *Série E*, **18**, 185-194.

[27] Houngue, H. (2018) Study of Silty Soils and Their Behavior in Tropical Environments: Case of Benin Roads. *Scientific Review of Construction*, **12**, 45-56.

[28] Centre Expérimental de recherches et d'Etudes du Bâtiment et des Travaux Publics (CEBTP) (1984) Guide pratique de dimensionnement des chaussées pour les pays tropicaux. In: *Guide Pratique de Dimensionnement des Chaussées Pour les Pays Tropicaux.*, 2ème Edition, La documentation française, 154 p.

[29] Philipponnat, G. and Hubert, B. (2016) Fondations et ouvrages en terre. Eyrolles.

[30] NF EN ISO 17892-5 (2017) Reconnaissance et essais géotechniques—Essais de laboratoire sur les sols—Partie 5: Essai de chargement par palier à l'œdomètre.

[31] CEBTP (2019) Revue du guide pratique de dimensionnement des chaussées pour les pays tropicaux. CEBTP.